
Article:
Dhimish, Mahmoud, d'Alessandro, Vincenzo and Daliento, Santolo (2022) Investigating the Impact of Cracks on Solar Cells Performance: Analysis based on Nonuniform and Uniform Crack Distributions. Industrial Informatics, IEEE Transactions on. pp. 1684-1693. ISSN: 1551-3203

https://doi.org/10.1109/TII.2021.3088721

Investigating the Impact of Cracks on Solar Cells Performance: Analysis based on Nonuniform and Uniform Crack Distributions

***Abstract*—The paper investigates the detrimental effect of nonuniform and uniform crack distributions over a solar cell in terms of open-circuit voltage (V_{oc}), short-circuit current density (J_{sc}), and output power, the latter under a wide range of irradiance conditions. The experimental procedure to detect the cracks relies on electroluminescence imaging, which is nondestructive and requires a relatively low amount of time. The Griddler software is adopted to translate the EL-taken image into V_{oc} and J_{sc} maps. The main findings can be summarized as follows: (i) the nonuniformly- and uniformly-cracked cells are both jeopardized in terms of output power; (ii) the loss corresponding to the cell with nonuniform distribution of cracks is increasingly higher than the uniformly-cracked counterpart as the irradiance hitting the cells grows, and (iii) all cells affected by nonuniform cracks are severely damaged in terms of fingers and rear busbar, which concur to limit the maximum output current.**

***Index Terms*—Cracks, electroluminescence (EL), open-circuit voltage, photovoltaic (PV), short-circuit current density, solar cells.**

I. INTRODUCTION

SOLAR cells often turn out to be affected by cracks during the manufacturing process when placing the junction or mounting the entire photovoltaic (PV) module [1]. Additionally, it was confirmed that the installation and shipping process leads to further cracks in the PV modules. In this Section, we aim to (i) present the research background in this field, including the most reliable techniques to detect the cracks, and (ii) discuss our contributions to knowledge.

A. Research Background

PV modules are exposed to multiple mechanical loads during their lifetime, including transport from production to the installation site, dust, snow, or high-wind volume. Felix *et al.* [2] presented a reliable, yet effective, 4-line bending setup to discover the most critical parameters determining solar cell cracks probability. They found that the mass-level, illumination-level, and solar cell stress factors are the key elements to determine the cracks. Even though this proposal is interesting, it requires a complicated procedure to follow, needing to dismount the modules and testing them with an indoor specialized testing facility.

To detect cracks in solar cells, the most reliable and used technique is the electroluminescence (EL) imaging. This technique can be managed in an outdoor environment, without dismounting the modules. The current is supplied to the module, and a proper CCD camera detects a radiative recombination of the yield carriers. It is advised to do the experimental work during the night to eliminate any distortion of the received emitted carriers [3].

The crack detection and localization through EL imaging cannot rely on the mere adoption of low-sensitivity CCD cameras. A significant effort has been made to improve and refine this technique. Yang *et al.* [4] proposed an advanced image fusion of EL images, which follows five vital steps and requires several seconds. An equivalent strategy was applied by Stromer *et al.* [5] with an improved solar cell cracks segmentation process based on the Vesselness filtering procedure. Another interesting method proposed by Dhimish *et al.* [6] exploits a digital-based algorithm called the "ORing method", by virtue of which the cracks size, location, orientation are more visible; at the same time, it takes up to 30 seconds to perform the calibration process. The same ORing method was also utilized by Dhimish & Mather [7], who further reduced the detecting and calibration time using an adjusted segmentation algorithm. The calibrated EL images can be processed within 0.1-0.3 seconds, excluding the EL imaging time, taking up to 5 seconds.

Other methods to detect solar cell cracks are based on deep learning models. Su *et al.* [8] used a novel complementary attention network to improve the EL detection of cracks in solar cells. They have found that out of 3629 images, nearly 2129 have detective areas. They also outlined that the percentage of the output power loss ranges from 0.2% to 12%, depending on the crack size. A similar deep learning model was also proposed by Rahman & Chen [9]; they have developed a multi-attention U-net (MAU-net) algorithm for solar cell cracks identification with a calibration time of 75 ms, excluding the EL imaging time.

Solar cell cracks could also be inspected using the photoluminescence (PL) imaging system [10]-[12]. The foremost disadvantages of the PL imaging systems require an expensive detection camera, and the excitation light might damage the solar cell emitted photons during the PL imaging procedure. Another crack detection relies on thermal cameras [13], [14]. The problem with these systems that the actual crack type, size and orientation cannot be identified, as only the heat-map of the solar cell can be obtained.

Today's research revealed that cracks in solar cells could decrease the output power in the formation of a loss in the short-circuit current density and the open-circuit voltage, even when using a maximum power point tracking (MPPT) unit, as stated by Seyedmahmoudian *et al.* [15]. A recent study conducted by Dhimish [16] shows that solar cell cracks (also referred to as µcracks) could reduce the output power of the cell in the range 0.9% to 42.8%, or even more, depending on the size of the crack. In addition, it was proven that the cracks can even lead to hot spots [16], [17]. In contrast with the above findings, other studies [18], [19] declare that there is a practically negligible output power loss in cracked solar cells. Hence, this detail requires additional evaluation using different assessment methods.

The way to increase the output power of cracked solar cells is using aggregate power electronics devices, such as a system-on-chip proposed by R. Gutierrez *et al.* [20]. Other approaches also suggest using neural-network-based control algorithms [21], [22].

B. Paper contributions and organization

In this paper, we will perform and discuss various experiments on solar cells affected by different types of cracks. The aim of the work is multi-fold and can be articulated as follows:

1) Experimentally evaluate the impact of two different types of cracks (nonuniform and uniform cracks distribution) on the open-circuit voltage, short-circuit current density, and the cells' output power.
2) Investigate the difference between the open-circuit voltage and the short-circuit current density of both cracks' types.
3) Analyze the output power of two cracked solar cell samples under low and high irradiance levels and compare the outcome with the theoretical predictions.

This paper is organized as follows. Section II presents the methodology, including the solar cell parameters and EL imaging. The results are shown in Section III, while a further comparative investigation of cracked solar cell samples is presented in Section IV. Section V details the electron microscopy analysis of cell samples affected by a nonuniform crack distribution. The conclusion is drawn in Section VI.

II. Methodology

This section aims to present the methodology adopted in this work, including the solar cell parameters and EL imaging.

A. Solar cell parameters

The main parameters used to describe the performance of solar cells are the open-circuit voltage (V_{oc}), short-circuit current density (J_{sc}), maximum output power (P_{max}), and fill factor (FF). All these parameters are determined by testing the solar cell under illumination. Theoretically, under standard test conditions (STC), where the solar irradiance is equal to 1000 W/m^2, the cell temperature is 25°C, and the spectrum resembles the AM1.5 one.

The V_{oc} represents the maximum voltage of the solar cell that can be produced when no current flows. The V_{oc} value depends on the saturation current density of the intrinsic cell diode (J_0) and the photo-generated current J_{ph} according to,

$$V_{oc} = \frac{K_B T}{q} \ln\left(\frac{J_{ph}}{J_0} + 1\right) \approx \frac{K_B T}{q} \ln\left(\frac{J_{ph}}{J_0}\right) \quad (1)$$

where K_B is Boltzmann constant, q is the elementary charge value, and T is the temperature in degrees Kelvin. Commercial or even lab-based solar cells typically have a V_{oc} above 500 mV [16], [23].

The J_{sc} represents the amount of current density that flows through the external circuit when the electrodes of the cell are short-circuited and depends on the photon flux incident on the surface of the cell. Hypothetically, the J_{sc} value for crystalline silicon solar cells is above 30 mA/cm^2 [23]. This value can be determined from the one-diode model as,

$$J_{sc} = J_{ph} - \frac{J_{sc} R_s}{R_{sh}} \quad (2)$$

where J_{ph} is the photo-generated current density, R_s is the series resistance, and R_{sh} is the shunt resistance.

As mentioned earlier, these two fundamental parameters will be compared for various cracked solar cells. The critical point is to emphasize that the drop in the V_{oc} does not necessarily results in a reduction in the J_{sc}, and vice-versa.

B. Electroluminescence imaging

The EL procedure, shown in Fig. 1, represents a valuable means to detect the location of cracks over solar cells. It is nondestructive and moderately fast, with computation times varying from 1 ms to a few seconds [9]. The EL system comprises a black environment to minimize the lights absorption whilst taking the EL images. In this work, the digital camera used to capture the images is a standard Nikon D40 with F-mount 18-55 mm lens. This camera has a spatial resolution of up to 63 µm on 156×156 mm cell sample and excellent near-IR sensitivity (1000-1100 nm).

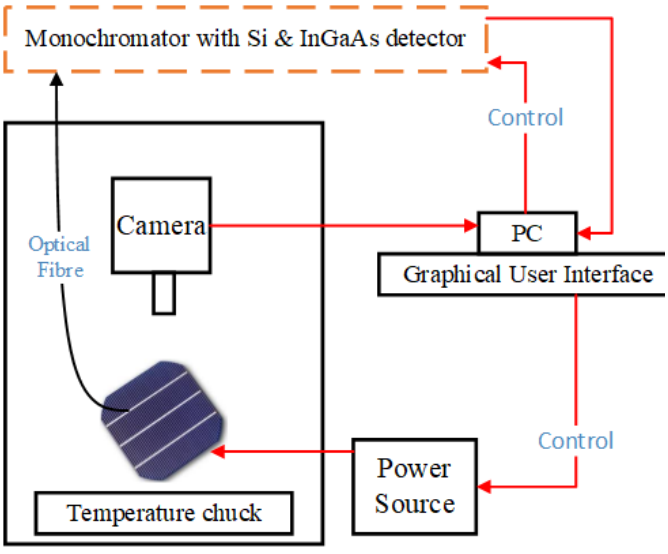

Fig. 1. Typical EL imaging procedure.

During the experimental stage, we have taken the EL images under J_{sc} condition. Simultaneously, the voltage biasing was at 0.7 V. The acquisition time was at least 2 minutes to ensure high-quality EL output images for every capture. The temperature of the controlled environment was equal to 25°C. It is worth noting that it is highly recommended to run the EL system by keeping the solar cell under test under the short-circuit conditions. However, according to Hu *et al.* [24], in this case, the test should not last a long time, as the output power performance of the cell could degrade.

The EL images were then processed using Griddler software to obtain the V_{oc} and J_{sc} distributions. We have also measured the current density vs. voltage (J-V) curves of every solar cell to quantify the output power losses. The J-V curves were obtained by a Keithley 2400 source meter under the illumination of AM 1.5, 100 mW/cm^2 provided by the CT50AAA solar simulator shown in Fig. 2. The solar simulator has a variable solar attenuation from 0 to 1.0 equivalent sun (0-1000 W/m^2). At maximum solar illumination, the temperature can also be controlled via the control system using LabVIEW software, to set at 25 ˚C.

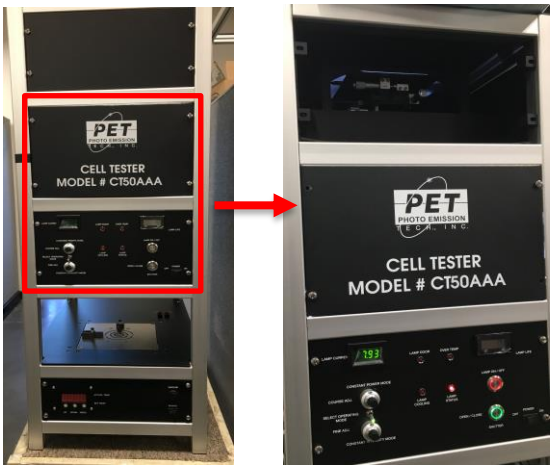

Fig. 2. CT50AAA solar simulator.

The summary of the experimental procedure followed in this work is presented in Fig. 3. First, the solar cell sample is adequately prepared to ensure that no surface damage or break-down occurs; then, an EL image is taken; lastly, the V_{oc} and J_{sc} maps are evaluated. Later, we observe the J-V curve for power loss analysis.

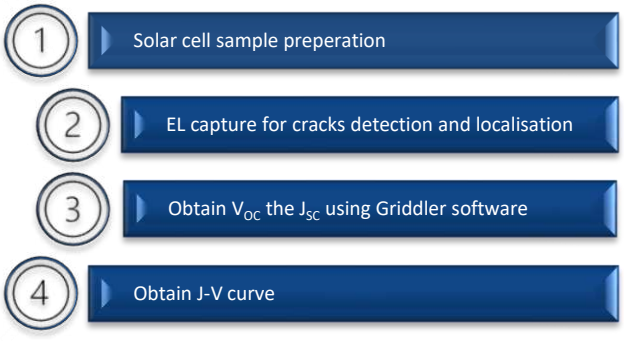

Fig. 3. Summary of the experimental procedure.

C. Electroluminescence output images

In Fig. 4, the EL images of two cell samples are presented. Fig. 4(a) shows a crack-free cell, while Fig. 4(b) shows a cell affected by an uneven distribution of cracks identified by the black areas. The three vertical lines represent the busbar.

For both samples, the original EL images are converted into V_{oc} and J_{sc} maps using a thermal-based imaging calibration process based on Griddler software. The J-V curves measured for both cells are reported in Fig. 4(c); it can be inferred that the external V_{oc} and J_{sc} of the cell suffering from cracks drop by 0.03 V and 5.83 mA/cm^2, respectively, compared to the crack-unaffected counterpart.

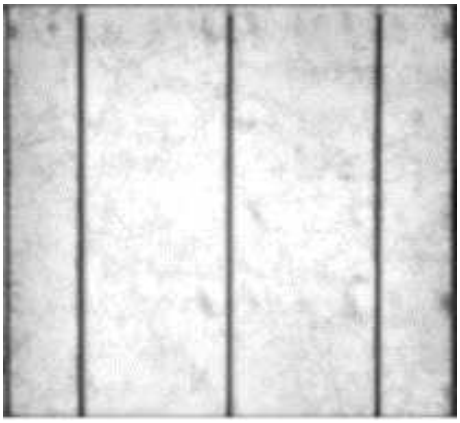

(a)

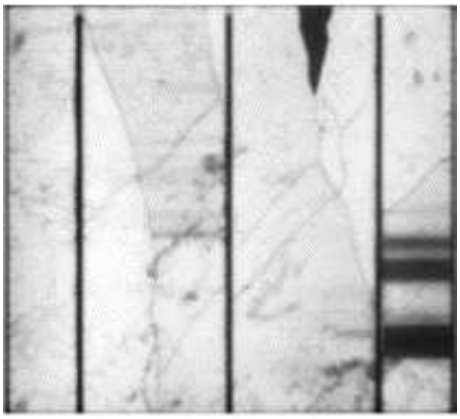

(b)

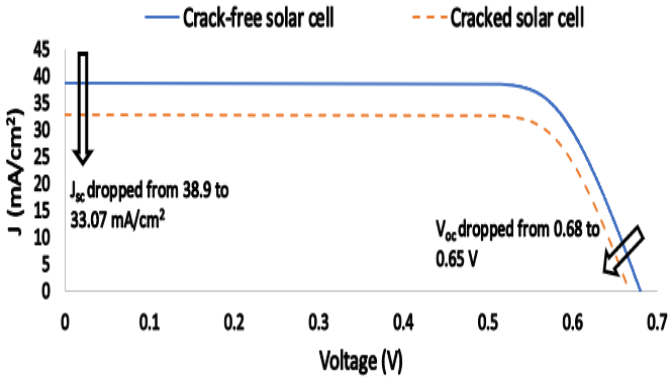

(c)

Fig. 4. EL images of (a) a crack-free. (b) a cracked solar cell. (c) corresponding experimental J-V curves.

III. Results and Discussion

In this section, we will present and discuss the analysis of two solar cells affected by different cracks distributions. The theoretical V_{oc} of the examined cells is equal to 0.68 V, and the J_{sc} is 38.9 mA/cm^2 under STC.

A. Nonuniform distribution of cracks

Let us consider the EL image reported in Fig. 5(a), which refers to a cell suffering from a markedly nonuniform crack distribution. From the inspection of the corresponding V_{oc} map obtained as shown in Fig. 5(b), it was found that the minimum V_{oc} in the cracked areas amounts to 0.54 V, which results in a percentage loss equal to 4.4% (calculated using equation (3)). This result confirms that cracks could locally reduce the V_{oc}.

$$Open-Circuit\ Front\ Voltage\ loss\ (\%) = \frac{Maximum\ V_{oc} - Minimum\ Measured\ V_{oc}\ of\ the\ Cracked\ Area}{Maximum\ V_{oc}} \times 100 = \frac{0.68-0.65}{0.68} \times 100 = 4.4\% \quad (3)$$

Fig. 5(c) illustrates the J_{sc} distribution. The minimum J_{sc} detected in the crack #1 area is equal to -54.7 mA/cm^2, while being -10.5 mA/cm^2 in the crack #2 region. The negative value of J_{sc} indicates a reverse current flowing, which obviously turns into a circumscribed overheating, i.e., a hot spot. Accordingly, the loss in the J_{sc} for both cracked areas is equal to (4) and (5). The cracked solar cell areas are significantly decreasing the J_{sc}.

$$\frac{Maximum\ J_{sc} - Measured\ J_{sc}\ of\ the\ Cracked\ Area}{Maximum\ J_{sc}} \times 100 = \frac{38.9-(-54.7)}{38.9} \times 100 = 240.6\% \quad (4)$$

$$J_{sc}\ loss\ for\ crack\ \#1\ (\%) = \frac{Maximum\ J_{sc} - Measured\ J_{sc}\ of\ the\ Cracked\ Area}{Maximum\ J_{sc}} \times 100 = \frac{38.9-(-10.5)}{38.9} \times 100 = 127\% \quad (5)$$

The results confirm that the J_{sc} drop over the cell can be drastically higher than the V_{oc} reduction; such an J_{sc} collapse is dictated by the localized increase in series resistance, which in turn depends on crack location, orientation, and size.

B. Uniform distribution of cracks

For a solar cell to be classified as uniformly affected by cracks, the cracks must be distributed evenly across the cell's surface, i.e., evenly affecting all locations between the busbars or a line-crack diagonally affecting the cell.

The EL image of a solar cell affected by a uniform distribution of cracks is presented in Fig. 6(a). In Fig. 6(b), it is evident that the consequently-even loss in V_{oc}, the lowest value of which is reached near the edges and amounts to 0.67 V (with a 1.47% reduction calculated by (6)).

$$Open-Circuit\ Front\ Voltage\ loss\ (\%) = \frac{Maximum\ V_{oc} - Minimum\ Measured\ V_{oc}\ of\ the\ Cracked\ Area}{Maximum\ V_{oc}} \times 100 = \frac{0.68-0.67}{0.68} \times 100 = 1.47\% \quad (6)$$

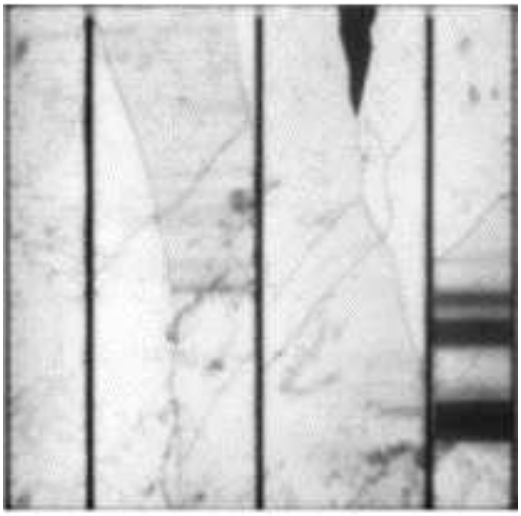

(a)

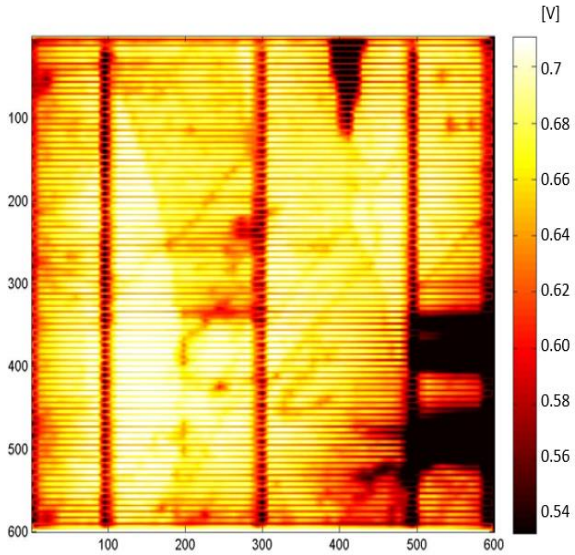

(b)

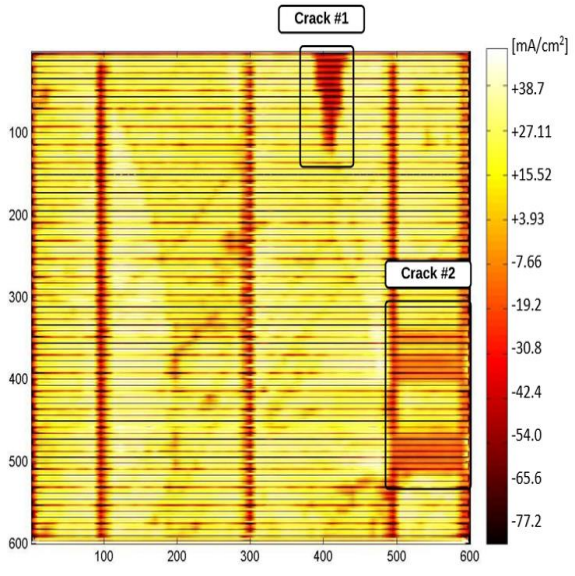

(c)

Fig. 5. Solar cell affected by a nonuniform distribution of cracks (a) EL image. (b) V_{oc}. (c) J_{sc} maps.

From Fig. 6(c), it is perceived that there is a uniform and marginal reduction of J_{sc} compared to the nonuniform crack distribution; this can be attributed to the lower localized increase of the series resistance. As an example, in the area labelled as "crack #1", the percentage reduction in J_{sc} is equal to 36.91 mA/cm^2, the J_{sc} loss of 5.1% is calculated using (7).

$$J_{sc}\ loss\ for\ crack\ \#1\ (\%) = \frac{Maximum\ J_{sc} - Measured\ J_{sc}\ of\ the\ Cracked\ Area}{Maximum\ J_{sc}} \times 100 = \frac{38.9-(36.91)}{38.9} \times 100 = 5.1\% \quad (7)$$

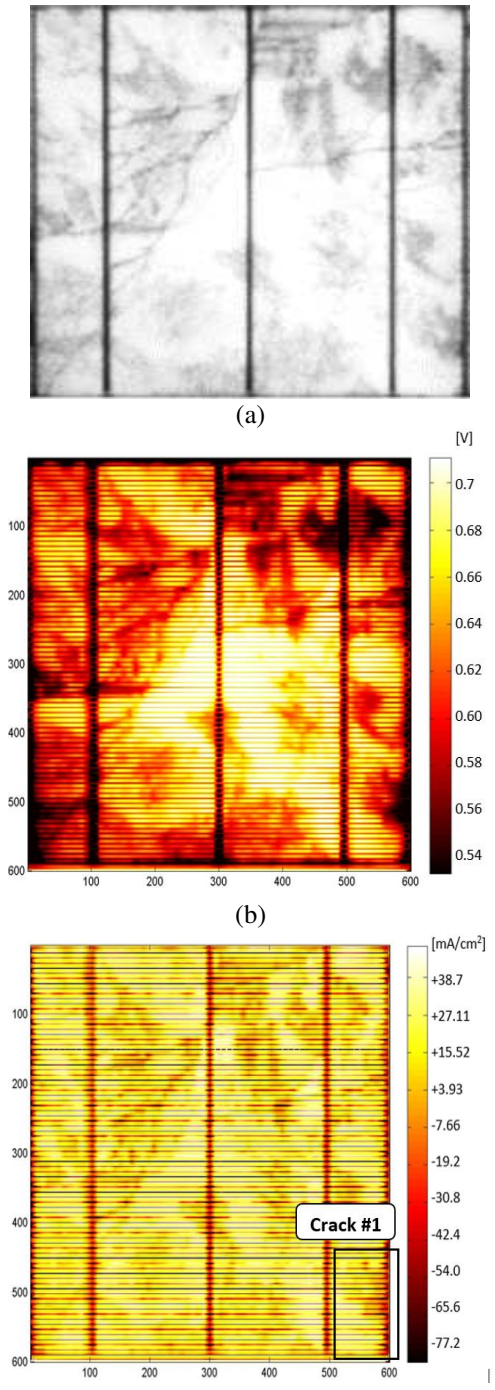

Fig. 6. Solar cell affected by a uniform distribution of cracks (a) EL image. (b) V_{oc}. (c) J_{sc} maps.

C. Output power losses (low to high irradiance testing)

The J-V curves measured for both cells at standard test conditions are shown in Fig. 7(a). As can be seen, the cell with a nonuniform distribution of crack suffers from a higher drop in terms of externally-measurable V_{oc} and J_{sc}.

As explained in Section I, it is still debated whether the presence of cracks leads to a drop in the yield output power or not. To tackle this issue, we show experimental results obtained for the solar cell samples affected by nonuniform and uniform crack distribution, illuminated under low to high (20 to 1000 W/m^2) levels of irradiance G at 25°C. The resulting output power as a function of G is shown in Fig. 7(b). As can be seen, (i) the cells suffer from insignificant losses compared to the theoretical value $0.0036\ G^{1.0392}$ at low irradiance levels (G≤200 W/m^2); (ii) for higher G values, both cells are impacted by a significant power loss, which grows with increasing G; (iii) the solar cell affected by a uniform distribution of cracks benefits from a higher output power. For G=1000 W/m^2, the power loss amounts to 2.55 and 2.02 W for the nonuniformly- and uniformly-cracked cells, respectively. The output power loss of both solar cells is calculated using (8) and (9).

$$output\ Power\ Loss\ "uniform\ crack\ solar\ cell" = Thoeretical\ Output\ Power - Measured\ Output\ Power = (0.0036\ G^{1.0392}) - (0.0049\ G^{0.9135}) = (0.0036 \times 1000^{1.0392}) - (0.0049 \times 1000^{0.9135}) = 2.02\ W \quad (8)$$

$$output\ Power\ Loss\ "nonuniform\ crack\ solar\ cell" = Thoeretical\ Output\ Power - Measured\ Output\ Power = (0.0036\ G^{1.0392}) - (0.0024\ G^{0.9851}) = (0.0036 \times 1000^{1.0392}) - (0.0024 \times 1000^{0.9851}) = 2.55\ W \quad (9)$$

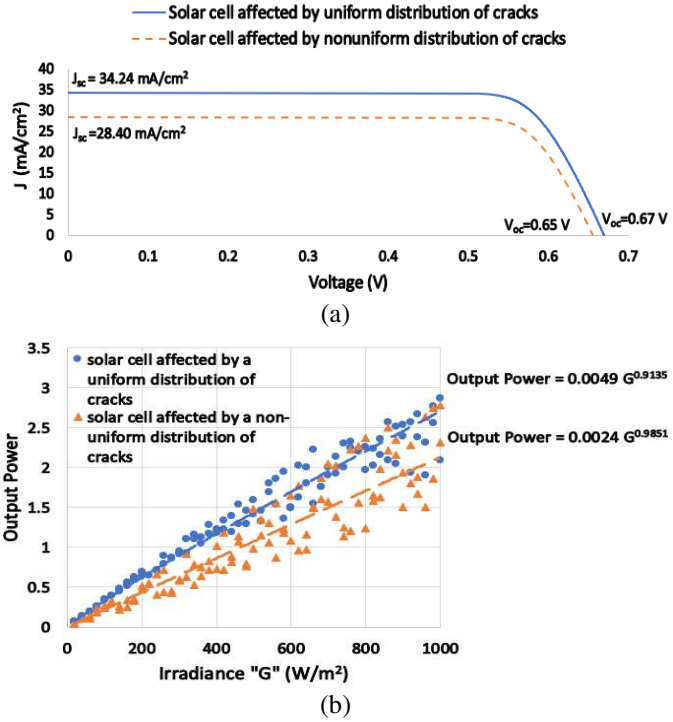

Fig. 7. (a) Measured J-V curve of the tested solar cell samples. (b) output power irradiance.

IV. Dataset of Other Cracked Solar Cell Samples: A Further Comparative Investigation

In this Section, the results shown and discussed earlier are supported by an extensive experimental campaign performed on additional cracked cells. More specifically, we have analyzed four samples affected by a nonuniform crack distribution (cells #1 to #4, shown in Fig. 8(a)) and four with a uniform crack distribution (cells #5 to #8 in Fig. 8(b)).

It can be inferred that the severity of the cracks increases from left to right, regardless of the distribution type. Hence, as far as the nonuniform type is concerned, we expect to have a more significant drop in the output power of cell #1 compared with cell #4, as cracks affect almost 75% of the first while being present only in circumscribed areas of the latter. In a similar fashion, for the uniform type, it is possible to identify cell #5 as the most impacted by cracks since the EL image is the darkest, which witnesses that the lowest number of emitted electrons was received.

These samples were illuminated by the CT50AAA solar simulator. The output power vs irradiance is presented in Fig. 9. For the samples with nonuniform cracks, the output power averaged along the entire irradiance range spans from 0.75 W (cell #1) to 1.33 W (cell #4), as indicated in Fig. 9(a). For the samples with uniform crack distribution, the average power varies from 1.21 W (cell #5) to 1.67 W (cell #8). Hence, the larger is the area affected by cracks; the higher is the decrease in output power.

It is worth mentioning that cells #5 and #6 show average powers (1.21 W and 1.35 W) similar to that of cell #4 (1.33 W). This result is somehow counterintuitive since the area affected by the crack distribution in cells #5 and #6 is much larger than that in cell #4, as can be simply inferred by looking at the EL images in Fig. 8. This evidences the fact that a nonuniform crack distribution more markedly jeopardizes the output power. An explanation of this phenomenon is given in Section V, where the solar cells affected by nonuniform cracks were analyzed using an electron microscope.

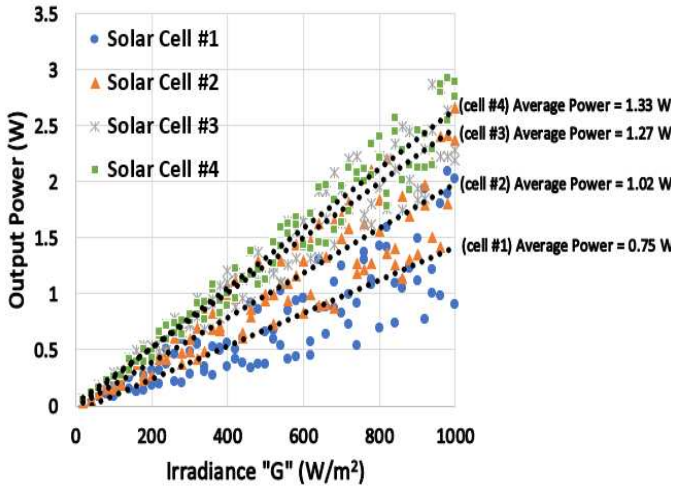

(a)

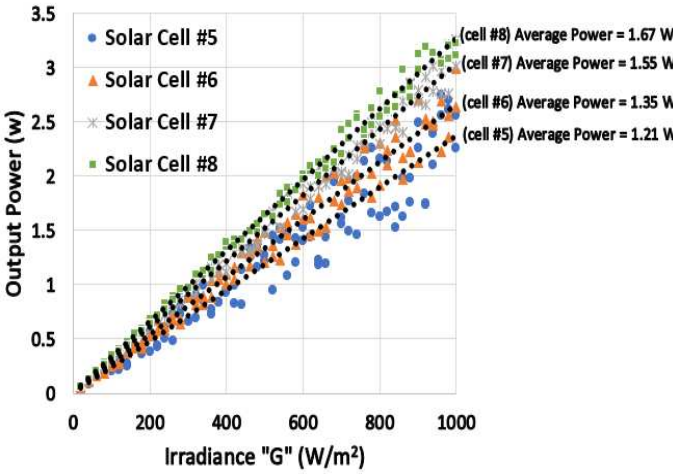

(b)

Fig. 9. Output power vs irradiance for (a) four cracked solar cell samples affected by a nonuniform crack distribution. (b) four cracked samples impacted by a uniform crack distribution.

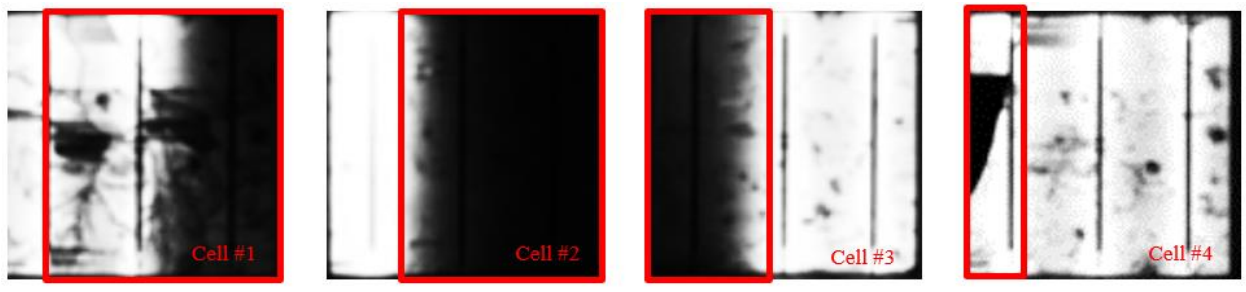

(a)

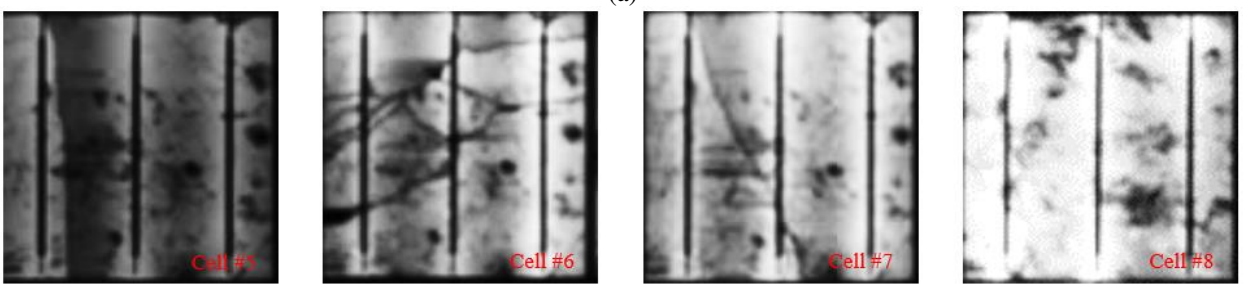

(b)

Fig. 8. EL images of solar cell samples affected by (a) nonuniform. (b) uniform crack distributions.

V. Investigating the Solar Cells Affected by Nonuniform Crack Distribution Under Electron Microscope

The electron microscopy (EM) technique illustrated in Fig. 10 was used to further examine the solar cells affected by nonuniform cracks (#1 to #4). The EM is interfaced with a PC using a data acquisition board. The acquisition of both the Everhart-Thornley Detector (ETD) and the Back Scatted Electron Diffraction (BSED) image can be acquired.

The EM testing allowed observing that in all cells, the cracks significantly impact the metallic fingers used to collect the generated current for delivery to the busbar, as witnessed by Fig. 11. In specific, a discontinuity of the finger connection was recognized, as shown in Fig. 11(a). It is evident that a discontinuity in the fingers necessarily leads to a drop in the output power [16], [18].

The second provocative observation that not only the front surface of the cells is affected by the severity of the nonuniform cracks, but also, we have remarked that the cracks constrained the rear busbar of the solar cells, as shown in Fig. 12. This would result in a limited generation capability of the solar cell even at standard testing conditions.

In summary, it is possible to conclude that the severe drop in the output power of the solar cells affected by a nonuniform crack distribution is also dictated by the damaged fingers and rear busbar.

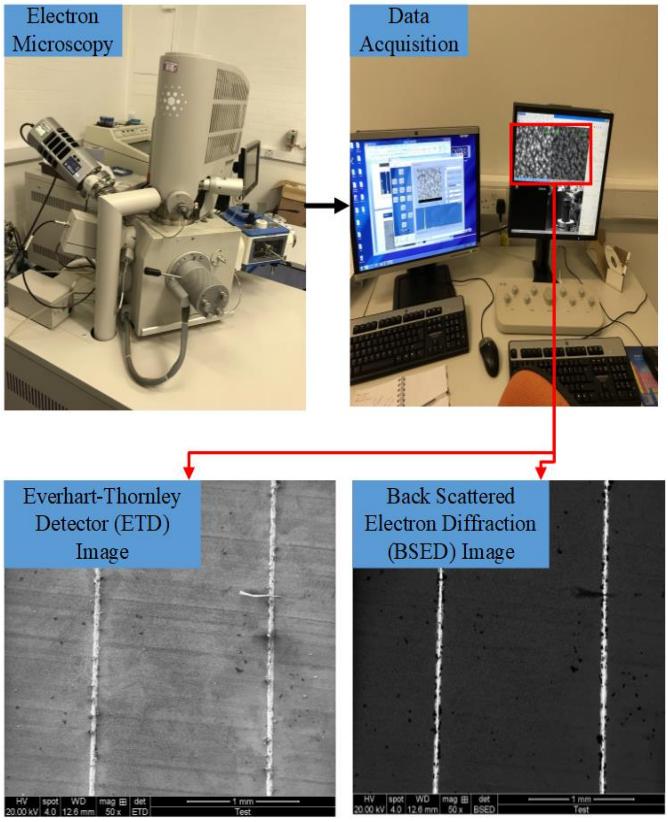

Fig. 10. Electron microscopy testing facility.

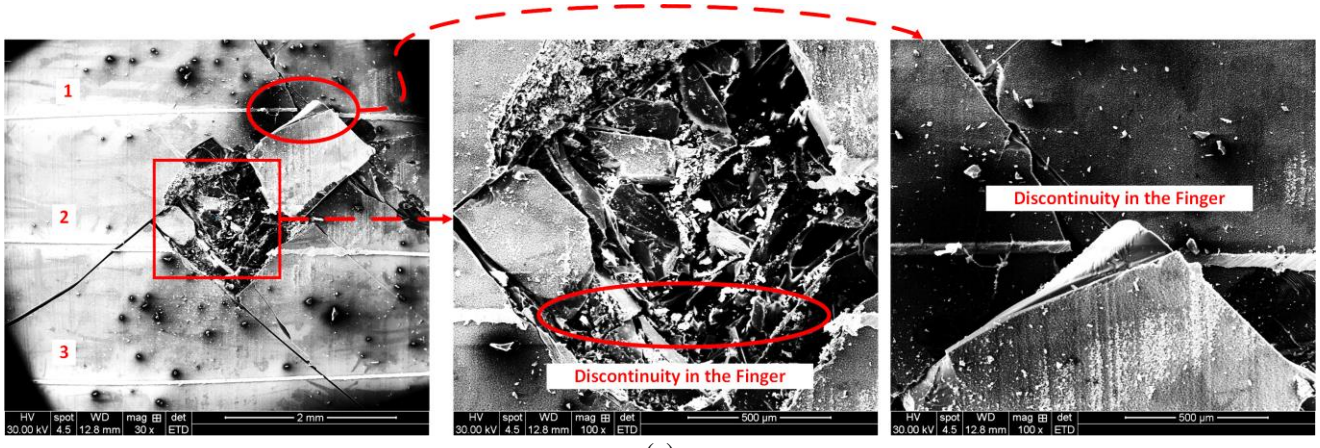

(a)

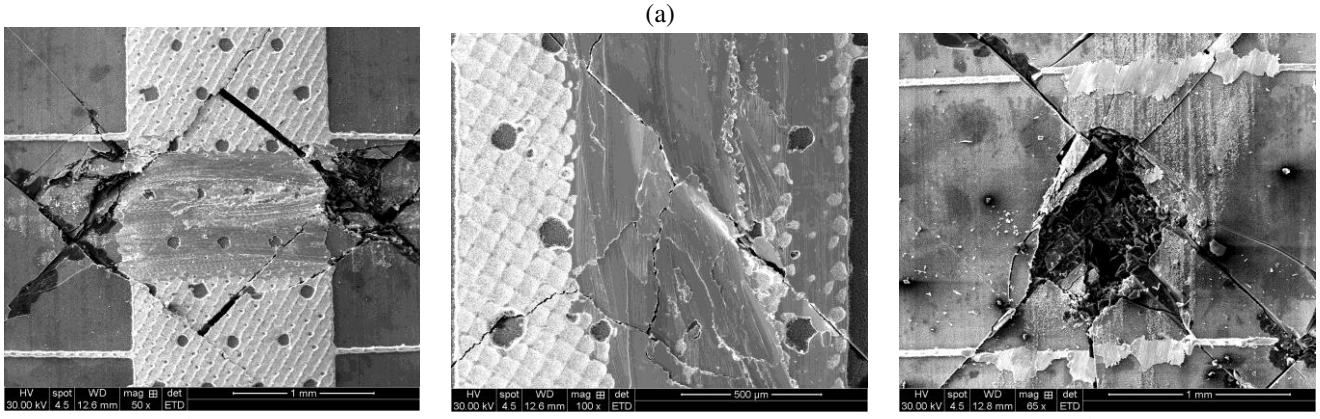

(b) (c) (d)

Fig. 11. Solar cell sample affected by a finger discontinuity (a) cell #1. (b) cell #2. (c) cell #3. (d) cell #4.

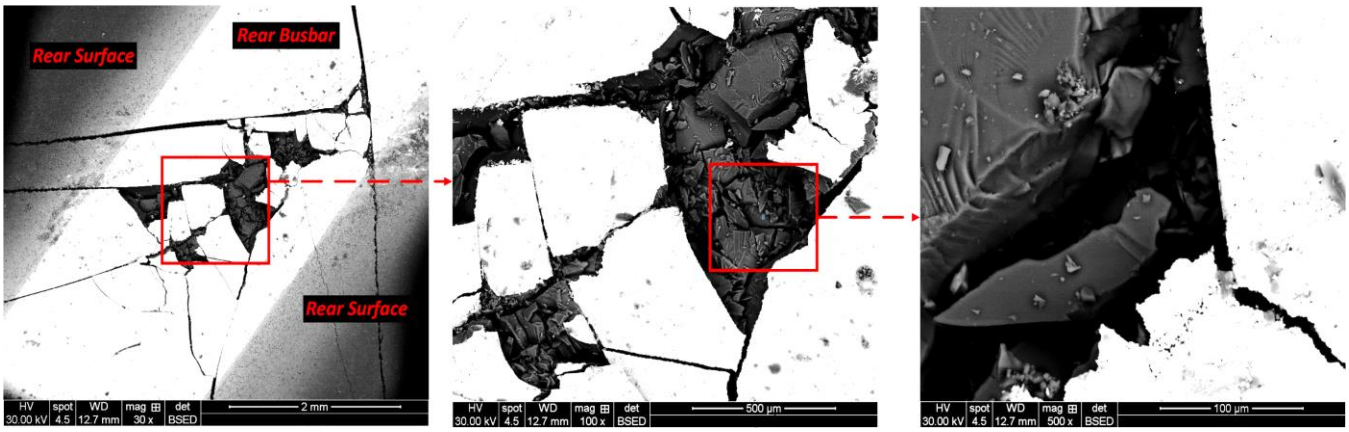

Fig. 12. Solar cell sample (cell #1) affected by cracked rear busbar.

VI. Conclusion

In this paper, we have analyzed various cracked solar cell samples using electroluminescence imaging, J-V curve measurements, and electron microscopy. The cells' degradation has been investigated in terms of open-circuit voltage, short-circuit current, and output power. We have found that cracks adversely affect output power production. Remarkably, we have observed that nonuniform cracks in solar cells lead to an additional reduction in the output power with respect to uniformly-cracked cells. The electron microscopy allowed discovering that all cells with nonuniform cracks are affected by severely damaged fingers and rear busbar, which concurs to limit the maximum achievable output current. This paper's main finding can be of interest to the photovoltaics industry, as a notable percentage of the products suffer from cracks related to the manufacturing process.

References

[1] D. P. Vasudevan, P. Bhatt, and A. Kottantharayil, "Impact of Transportation on Indian Roads, on PV Modules," *2019 IEEE 46th Photovoltaic Specialists Conference (PVSC)*, Chicago, IL, USA, 2019, pp. 1529-1532, doi: 10.1109/PVSC40753.2019.8980720.

[2] F. Haase, J. Käsewieter, S. R. Nabavi, E. Jansen, R. Rolfes, and M. Köntges, "Fracture Probability, Crack Patterns, and Crack Widths of Multicrystalline Silicon Solar Cells in PV Modules During Mechanical Loading," *IEEE Journal of Photovoltaics*, vol. 8, no. 6, pp. 1510-1524, Nov. 2018, doi: 10.1109/JPHOTOV.2018.2871338.

[3] M. Dhimish and P. Mather, "Development of Novel Solar Cell Micro Crack Detection Technique," *IEEE Transactions on Semiconductor Manufacturing*, vol. 32, no. 3, pp. 277-285, Aug. 2019, doi: 10.1109/TSM.2019.2921951.

[4] R. Yang *et al.*, "Electromagnetic Induction Heating and Image Fusion of Silicon Photovoltaic Cell Electrothermography and Electroluminescence," *IEEE Transactions on Industrial Informatics*, vol. 16, no. 7, pp. 4413-4422, Jul. 2020, doi: 10.1109/TII.2019.2922680.

[5] D. Stromer, A. Vetter, H. C. Oezkan, C. Probst, and A. Maier, "Enhanced Crack Segmentation (eCS): A Reference Algorithm for Segmenting Cracks in Multicrystalline Silicon Solar Cells," *IEEE Journal of Photovoltaics*, vol. 9, no. 3, pp. 752-758, May 2019, doi: 10.1109/JPHOTOV.2019.2895808.

[6] M. Dhimish, V. Holmes and P. Mather, "Novel Photovoltaic Micro Crack Detection Technique," *IEEE Transactions on Device and Materials Reliability*, vol. 19, no. 2, pp. 304-312, Jun. 2019, doi: 10.1109/TDMR.2019.2907019.

[7] M. Dhimish and P. Mather, "Ultrafast High-Resolution Solar Cell Cracks Detection Process," *IEEE Transactions on Industrial Informatics*, vol. 16, no. 7, pp. 4769-4777, Jul. 2020, doi: 10.1109/TII.2019.2946210.

[8] B. Su, H. Y. Chen, P. Chen, G. Bian, k. Liu, and W. Liu, "Deep Learning-based Solar-Cell Manufacturing Defect Detection with Complementary Attention Network," *IEEE Transactions on Industrial Informatics*, early access, doi: 10.1109/TII.2020.3008021.

[9] M. R. U. Rahman and H. Chen, "Defects Inspection in Polycrystalline Solar Cells Electroluminescence Images Using Deep Learning," *IEEE Access*, vol. 8, pp. 40547-40558, 2020, doi: 10.1109/ACCESS.2020.2976843.

[10] R. Duru *et al.*, "Photoluminescence Imaging for Buried Defects Detection in Silicon: Assessment and Use-Cases," *IEEE Transactions on Semiconductor Manufacturing*, vol. 32, no. 1, pp. 23-30, Feb. 2019, doi: 10.1109/TSM.2018.2871967.

[11] Y. Zhu, F. D. Heinz, M. Juhl, M. C. Schubert, T. Trupke, and Z. Hameiri, "Photoluminescence Imaging at Uniform Excess Carrier Density Using Adaptive Nonuniform Excitation," *IEEE Journal of Photovoltaics*, vol. 8, no. 6, pp. 1787-1792, Nov. 2018, doi: 10.1109/JPHOTOV.2018.2869541.

[12] S. Ying, B. Chen, and W. Tseng, "Thin-Film Luminescent Solar Concentrators Using Inorganic Phosphors," *IEEE Transactions on Electron Devices*, vol. 66, no. 5, pp. 2290-2294, May 2019, doi: 10.1109/TED.2019.2908683.

[13] L. Xia, Z. Wen, K. Liao, J. Chen, Q. Li, and X. Luo, "Unveiling the Failure Mechanism of Electrical Interconnection in Thermal-Aged PV Modules," *IEEE Transactions on Device and Materials Reliability*, vol. 20, no. 1, pp. 24-32, Mar. 2020, doi: 10.1109/TDMR.2019.2956506.

[14] Y. He, B. Du, and S. Huang, "Noncontact Electromagnetic Induction Excited Infrared Thermography for Photovoltaic Cells and Modules Inspection," *IEEE Transactions on Industrial Informatics*, vol. 14, no. 12, pp. 5585-5593, Dec. 2018, doi: 10.1109/TII.2018.2822272.

[15] M. Seyedmahmoudian, T. K. Soon, B. Horan, A. Ghandhari, S. Mekhilef, and A. Stojcevski, "New ARMO-based MPPT Technique to Minimize Tracking Time and Fluctuation at Output of PV Systems under Rapidly Changing Shading Conditions," *IEEE Transactions on Industrial Informatics*, early access, doi: 10.1109/TII.2019.2895066.

[16] M. Dhimish, "Micro cracks distribution and power degradation of polycrystalline solar cells wafer: Observations constructed from the analysis of 4000 samples," *Renewable Energy*, vol. 145, pp. 466-477, Jan. 2020, doi: 10.1016/j.renene.2019.06.057.

[17] K. Yang, Y. Wu, and F. Huang, "Microcrack and microvoid dominated damage behaviors for polymer bonded explosives under different dynamic loading conditions," in *Mechanics of Materials*, vol. 137, pp. 1031130, Oct. 2019, doi: 10.1016/j.mechmat.2019.103130.

[18] L. Papargyri , M. Theristis, B. Kubicek, T. Krametz, C. Mayr, P. Papanastasiou, and G. E. Georghiou, "Modelling and experimental investigations of microcracks in crystalline silicon photovoltaics: A review," in *Renewable Energy*, vol. 145, pp. 2387-2408, Jan. 2020, doi: 10.1016/j.renene.2019.07.138.

[19] G.C. Eder, Y. Voronko, G. Oreski, W. Mühleisen, M. Knausz, A. Omazic, A. Rainer, C. Hirschl, and H. Sonnleitner, "Error analysis of aged modules with cracked polyamide backsheets," in *Solar Energy*, vol. 203, pp. 110194, Dec. 2019, doi: 10.1016/j.solmat.2019.110194.

[20] R. Gutiérrez, J. M. Blanes, D. Marroquí, A. Garrigós, and F. J. Toledo, "System-on-Chip for Real-Time Satellite Photovoltaic Curves Telemetry," in *IEEE Transactions on Industrial Informatics*, vol. 14, no. 3, pp. 951-957, Mar. 2018, doi: 10.1109/TII.2017.2755463.

[21] P. Shukl and B. Singh, "Delta-Bar-Delta Neural-Network-Based Control Approach for Power Quality Improvement of Solar-PV-Interfaced Distribution System," *IEEE Transactions on Industrial Informatics*, vol. 16, no. 2, pp. 790-801, Feb. 2020, doi: 10.1109/TII.2019.2923567.

[22] Q. Zou, Z. Zhang, Q. Li, X. Qi, Q. Wang, and S. Wang, "DeepCrack: Learning Hierarchical Convolutional Features for Crack Detection," in *IEEE Transactions on Image Processing*, vol. 28, no. 3, pp. 1498-1512, March 2019, doi: 10.1109/TIP.2018.2878966.

[23] A. Tyagi, K. Ghosh, A. Kottantharayil, and S. Lodha, "An Analytical Model for the Electrical Characteristics of Passivated Carrier- Selective Contact (CSC) Solar Cell," *IEEE Transactions on Electron Devices*, vol. 66, no. 3, pp. 1377-1385, Mar. 2019, doi: 10.1109/TED.2019.2893998.

[24] X. Hu *et al.*, "Resistive Effects on the Spatially Resolved Absolute Electroluminescence of Thin-Film Cu(In, Ga)Se2 Solar Cells Studied by a Distributed Two-Diode Model," *IEEE Access*, vol. 8, pp. 112859-112866, 2020, doi: 10.1109/ACCESS.2020.3002659.